Article

TRANSPARENT PROCESS

THE EMBO JOURNAL

Cyclin O (*Ccno*) functions during deuterosome-mediated centriole amplification of multiciliated cells

Maja C Funk[1,2], Agata N Bera[1,3], Tabea Menchen[4], Georg Kuales[1], Kerstin Thriene[5], Soeren S Lienkamp[1,3], Jörn Dengjel[3,5], Heymut Omran[4], Marcus Frank[6] & Sebastian J Arnold[1,3,*]

Abstract

Mucociliary clearance and fluid transport along epithelial surfaces are carried out by multiciliated cells (MCCs). Recently, human mutations in *Cyclin O* (*CCNO*) were linked to severe airway disease. Here, we show that *Ccno* expression is restricted to MCCs and the genetic deletion of *Ccno* in mouse leads to reduced numbers of multiple motile cilia and characteristic phenotypes of MCC dysfunction including severe hydrocephalus and mucociliary clearance deficits. Reduced cilia numbers are caused by compromised generation of centrioles at deuterosomes, which serve as major amplification platform for centrioles in MCCs. *Ccno*-deficient MCCs fail to sufficiently generate deuterosomes, and only reduced numbers of fully functional centrioles that undergo maturation to ciliary basal bodies are formed. Collectively, this study implicates CCNO as first known regulator of deuterosome formation and function for the amplification of centrioles in MCCs.

Keywords *Ccno*; centriole amplification; deuterosomes; mouse; multiciliated cells

Subject Categories Cell Adhesion, Polarity & Cytoskeleton; Development & Differentiation; Molecular Biology of Disease

DOI 10.15252/embj.201490805 | Received 20 July 2014 | Revised 23 January 2015 | Accepted 27 January 2015 | Published online 23 February 2015

The EMBO Journal (2015) 34: 1078–1089

Introduction

Cilia are microtubule-based, hairlike organelles that protrude from the surfaces of cells and are present in the majority of animal phyla (Carvalho-Santos *et al*, 2011). While most cells possess one cilium, then referred to as primary cilium, specialized epithelial cells can generate up to several hundred cilia on their surface, then referred to as multiciliated cells (MCCs). Cilia of MCCs exhibit coordinated beating motility that creates a directional flow enabling fluid transport along epithelial surfaces (Fliegauf *et al*, 2007). Fluid flow directs the distribution of signalling molecules, or generates mechanical forces for fluid transportation, as found in the ventricular system of the brain. Additionally, fluid flow is essential for the clearance of environment-exposed epithelia by mucus transport, such as in the respiratory tract epithelium.

Human individuals with congenital ciliary motility disorders present with clinical features of recurrent airway infections, infertility, situs ambiguous and increased incidence of hydrocephalus, collectively referred to as primary ciliary dyskinesia (PCD) (reviewed by Knowles *et al*, 2013). Recently, human cases of congenital mucociliary clearance disorders with predominant respiratory symptoms have been reported that are primarily caused by the reduced generation of multiple motile cilia (RGMC) (Wallmeier *et al*, 2014). Mutations in the *CCNO* gene lead to the compromised generation of sufficient cilia numbers on MCCs, while the beating motility of remaining cilia is not generally disrupted (Wallmeier *et al*, 2014). This study suggested requirements of CCNO function for docking of centrioles to the apical cell membrane. However, a more detailed analysis of CCNO function during the generation of multiple motile cilia may reveal alternative roles of CCNO for cilia biogenesis in MCCs.

During ciliogenesis, centrioles dock to the plasma membrane, thereby forming basal bodies, which serve as platform for the outgrowth of ciliary axonemes (reviewed by Nigg & Raff, 2009). While in monociliated cells the cilium extends from the former mother centriole, MCCs massively amplify centrioles as initiating event of multiciliogenesis (Sorokin, 1968). Two alternative modes of centriole amplification have been described based on ultrastructural studies (Sorokin, 1968). In the canonical pathway of centriole amplification, several procentrioles form in association with the mother centriole, denoted as the mother-centriole-dependent pathway (MCD). Additionally, the massive amplification of centrioles is achieved in a mother-centriole-independent, acentriolar fashion at

1 University Medical Centre, Renal Department, Centre for Clinical Research, Freiburg, Germany
2 Spemann Graduate School of Biology and Medicine, Freiburg, Germany
3 BIOSS Centre of Biological Signalling Studies, Albert-Ludwigs-University, Freiburg, Germany
4 Department of Pediatrics, University Hospital Muenster, Muenster, Germany
5 Department of Dermatology, ZBSA Centre for Biological Systems Analysis, Medical Centre, University of Freiburg, Freiburg, Germany
6 Medical Biology and Electron Microscopy Centre, University Medicine Rostock, Rostock, Germany
*Corresponding author. Tel: +49 761 270 63120; E-mail: sebastian.arnold@uniklinik-freiburg.de

so-called deuterosomes (deuterosome-dependent pathway, DD). These serve as additional procentriole nucleation centres and are specific for MCCs (Sorokin, 1968). A recent study has demonstrated that deuterosomes are generated in a consecutive manner strictly from daughter centrioles, implicating that predominantly daughter centrioles contribute to centriole amplification in MCCs (Al Jord *et al*, 2014). Previously, deuterosomes were solely described by their characteristic strongly electron-dense, ring-like appearance in transmission electron microscopy and until recently their composition was unknown (Sorokin, 1968). Two studies have elucidated some molecular components of deuterosomes by the identification of DEUP1 and CCDC78 as proteins that specifically localize to deuterosomes, but not to the foci of mother centrioles during procentriole formation (Klos Dehring *et al*, 2013; Zhao *et al*, 2013). Forced expression of *Deup1* leads to amplification of centrioles, and bacterially expressed, recombinant DEUP1 forms spherical structures reminiscent of deuterosomes in MCCs (Zhao *et al*, 2013). To date, the knowledge about regulation of deuterosome formation, number and control of their function during centriole amplification remains limited. However, two recent studies have identified the transcription factor MULTICILIN (*Mcidas*) as direct and broad regulator of the transcriptional programme responsible for DD-ciliogenesis in MCCs, including the positive regulation of *Ccno* (Ma *et al*, 2014). Additionally, it is assumed that centriole formation via deuterosomes is at least partially controlled by the same set of known factors for centriole biogenesis of cycling cells, such as PLK4 (Kleylein-Sohn *et al*, 2007), SAS-6 (Strnad *et al*, 2007) and CEP152 (Blachon *et al*, 2008). However, the precise roles of these players have yet to be identified in MCCs (Tang, 2013).

In this study, we describe highly MCC-specific expression of *Ccno* from early phases of centriole amplification and ciliogenesis during embryonic development and in differentiating MCCs in culture. Using targeted genetics, we analysed *Ccno*-deficient mice, which show characteristics of PCD-like phenotypes, as a result of significantly reduced cilia numbers of MCCs. Impaired ciliogenesis of *Ccno*-deficient MCCs is caused by functional defects of deuterosome-mediated centriole amplification. Reduced numbers of deuterosomes are formed and newly generated centrioles exhibit defects of maturation and localization, resulting in reduced numbers of properly docked and fully functional ciliary basal bodies. However, *Ccno* does not seem to impact on the MCD mode of centriole amplification. In summary, we demonstrate that *Ccno* plays critical roles in the regulation of deuterosome formation and function, required for amplification of functional centrioles and thus the generation of multiple motile cilia in MCCs.

Results

Ccno is specifically expressed in MCCs and the embryonic node

In an expression screen that aimed for identifying transcripts with regional specific expression during cell lineage formation in the embryonic day 7.5 (E7.5) mouse embryo, we discovered highly regional specific transcription of the *Ccno* gene in cells of the most anterior tip of the primitive streak and in the embryonic node (Fig 1A). The node is the transient organizing structure that establishes the left-right body axis in a cilia-dependent manner. Pit cells in the centre of the node carry motile monocilia that generate a leftward fluid flow across the ventral node surface, required for establishing left-right asymmetry of the body axis (Shiratori &

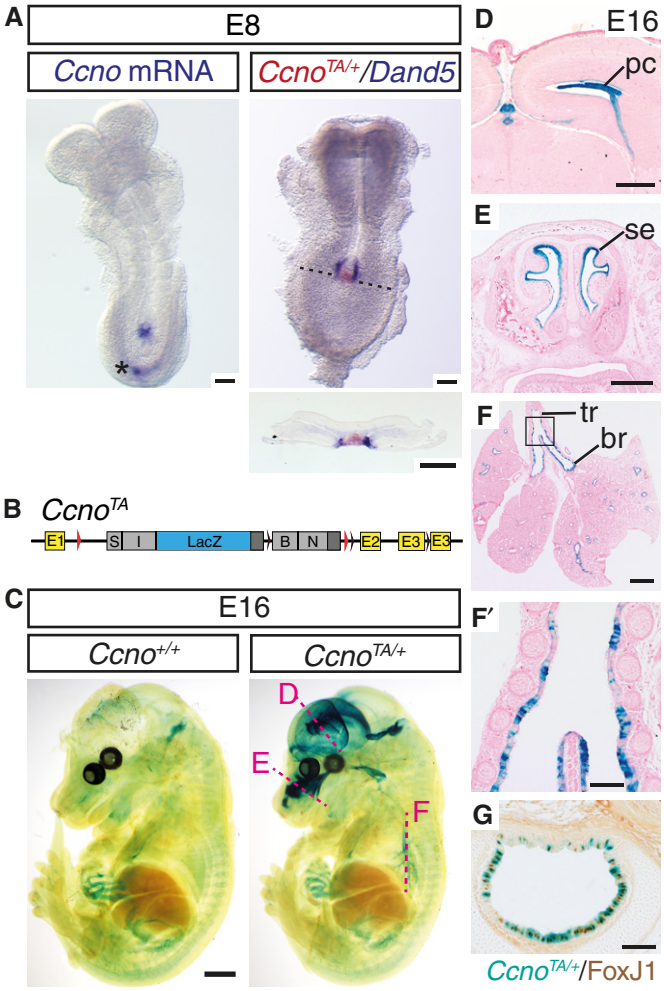

Figure 1. *Ccno* is specifically expressed in multiciliated cells and the embryonic node.

A *Ccno* mRNA is expressed in the embryonic node at E8 as shown by *in situ* hybridization. Occasionally, additional expression is observed at the posterior tip of the embryo (asterisk). Double labelling by staining for *LacZ* expression from the $Ccno^{TA}$ allele (shown in B) and *in situ* hybridization for *Dand5*, marking crown cells at the circumference of the node. *Ccno* expression is restricted to ciliated, ventral pit cells of the node as detailed in the transverse section at the indicated plane.

B Schematic of the $Ccno^{TA}$ targeted *LacZ* knock-in allele used in (A) and (C–G).

C Whole embryo X-Gal staining of E16 $Ccno^{TA/+}$ and wild-type control embryos and indicated section planes of (D–F').

D–F' Histological sections of LacZ-stained $Ccno^{TA/+}$ embryo at E16 reveal *Ccno* expression in the epithelium of (D) plexus choroideus and ependyme, (E) snout epithelium, and (F, F') trachea and bronchi. pc, plexus choroideus; se, snout epithelium; tr, trachea; and br, bronchus.

G Co-expression of *Ccno* and *Foxj1* in multiciliated cells of the trachea shown by double staining for X-Gal and immunohistochemistry using a FOXJ1-specific antibody.

Data information: Scale bars: 100 μm in (A), 1 mm in (C), 500 μm in (D-F') and 100 μm in (G).

Hamada, 2006). *Ccno* expression was exclusively found in pit cells, but was excluded from the crown cells that constitute the margins of the node and carry non-motile cilia (Fig 1A).

For the robust detection of *Ccno* gene expression, we established a reporter mouse line by blastocyst injection of ES cells generated by the EUCOMM consortium (Skarnes *et al*, 2011), which carry a *LacZ* reporter allele in intron 1 of the *Ccno* gene (Fig 1B and Supplementary Fig S1A). *LacZ* expression from this $Ccno^{LacZ}$ reporter allele (referred to as $Ccno^{TA}$ hereafter) recapitulates endogenous mRNA expression (Fig 1A and Supplementary Fig S1C) and was used for successive analyses of *Ccno* expression. At later stages of development, *Ccno* expression was restricted to epithelial tissues that share as common feature the presence of multiciliated cells (MCCs) (Fig 1C). *Ccno*-expressing epithelia include the ependymal epithelium lining the ventricular surfaces of the brain (Fig 1C), the plexus choroideus within the ventricular lumen (Fig 1D), and the epithelium of the upper (snout epithelium; Fig 1E) and lower respiratory tract (trachea and bronchi, Fig 1F). Expression analysis in tracheal epithelium revealed co-expression of *Ccno* and *Foxj1*, a key transcriptional regulator for the generation of motile cilia (Fig 1G) (Chen *et al*, 1998; Brody *et al*, 2000). Collectively, these expression patterns suggest specific functions of *Ccno* in MCCs.

Ccno deletion in mouse causes functional defects of MCCs due to reduced cilia number

To study *Ccno* gene function, we generated mice with a targeted deletion at the *Ccno* gene locus by crossing $Ccno^{TA/+}$ animals to the transgenic *Sox2*::*Cre* germline deleter strain (Hayashi *et al*, 2002) (Supplementary Fig S1A). The deletion of coding exons 2 and 3 resulted in a *Ccno* null allele configuration (referred to as $Ccno^{RA}$ hereafter). To generate homozygous deletions of the *Ccno* gene locus, we intercrossed $Ccno^{RA/+}$ heterozygous animals. $Ccno^{RA/RA}$ mice were born, however were not represented at Mendelian ratio (25%) at weaning age (postnatal day 21; P21). Instead, only 14% of $Ccno^{RA/RA}$ homozygously deleted mutants could be observed (35/246; Fig 2E), while $Ccno^{RA/RA}$ embryos were found at expected frequency of 25% until E17 (Fig 2E), indicating perinatal lethality until P21 in *Ccno*-deficient offspring. From the remaining $Ccno^{RA/RA}$ mice, ~57% (20/35) developed a prominent hydrocephalus, leading to abnormal head morphology (Fig 2A and B) and growth retardation. MRI analysis and dissected brains revealed massively enlarged ventricles and a substantial thinning of the cerebral cortex (Fig 2B and C). All $Ccno^{RA/RA}$ animals that developed severe hydrocephalus died within the first 6 weeks of life. Remaining $Ccno^{RA/RA}$ homozygous animals (15/35, 43%) appeared grossly normal and did not suffer from untimely lethality (Fig 2E). Importantly, no obvious signs of laterality defects in *Ccno*-deficient embryos or adult animals, and no sneezing or coughing were observed. Male and female animals that were not severely affected by hydrocephalus were fertile at maturity age when used for breeding.

Hydrocephalus in mice is frequently caused by defective ciliary function of ependymal MCCs leading to the reduced intraventricular transport of cerebrospinal fluid (reviewed by Lee, 2013). To investigate additional manifestations associated with disturbed MCC function, we examined paranasal cavities by mucus staining of $Ccno^{RA/RA}$ animals. Obvious mucosal congestion was found in paranasal cavities of all examined $Ccno^{RA/RA}$ animals ($n = 3$), but not in control littermates from the same cage ($n = 3$) (Fig 2D and D'). The predominant manifestation of MCC dysfunction in human individuals is insufficient airway clearance leading to recurrent airway infections. Histologicalanalysis of adult *Ccno*-deficient lung tissue did not reveal signs of inflammation or mucus congestions of $Ccno^{RA/RA}$ mice that were maintained in a specific pathogen-free environment (Supplementary Fig S2A and B). However, scanning electron microscopy (SEM) of tracheal epithelium from $Ccno^{RA/RA}$ adult mice showed a pronounced reduction of cilia number on the surface of tracheal MCCs (Fig 2F and F'). In comparison to wild-types, cilia of *Ccno*-deficient MCCs appeared less grouped and extended mostly from the central regions of the apical cell surface, leaving the margins of MCCs undecorated (Fig 2F and F'). Otherwise, single cilia did not show gross morphological abnormalities and the overall cell number of MCCs appeared unchanged (Fig 2F). Immunofluorescence (IF) staining of adult $Ccno^{RA/RA}$ tracheal epithelium for acetylated α-tubulin, which marks ciliary axonemes, similarly showed reduced staining in accordance with overall reduced number of cilia (Supplementary Fig S2D). The presence of the motor protein dynein outer arm heavy chain 5 (DNAH5) suggested that remaining cilia are motile (Supplementary Fig S2D') (Fliegauf *et al*, 2005). This assumption was confirmed by video microscopy of tracheal epithelium that revealed ciliary motility of remaining cilia on *Ccno*-deficient MCCs (Supplementary Movies S1 and S2).

To uncover ultrastructural details of MCCs, we employed transmission electron microscopy (TEM) of adult tracheal epithelium. Confirming the results from SEM and IF analyses, TEM also revealed considerably reduced numbers of cilia in *Ccno*-deficient MCCs (Fig 2G). Instead of properly docked basal bodies, we observed multiple mislocalized and misshaped basal bodies that failed to correctly dock to the apical plasma membrane and to extend ciliary axonemes (Supplementary Fig S3B–E). Additionally, the cytoplasm of *Ccno*-deficient cells frequently contained electron-dense structures that most likely represent remnants of microtubular-based organelles such as centrioles and/or basal bodies (Fig 2G and Supplementary Fig S3B–E). Ultrastructural analysis of the few cilia that extend from correctly docked basal bodies showed pleiotropic axonemal defects at increased frequencies (Supplementary Fig S3H–J). These included microtubular alterations, such as singlet (Supplementary Fig S3H), or triplet microtubules (Supplementary Fig S3I), abnormal microtubule doublet number and lack of the central tubule pair (Supplementary Fig S3J). However, also axonemes with normal morphology were observed (Supplementary Fig S3G), likely explaining conservation of some ciliary beating motility that could be seen in *Ccno*-deficient tracheal epithelium (Supplementary Movies S1 and S2).

Dynamic expression of *Ccno* suggests roles during early stages of ciliogenesis

To examine if the observed ciliary defects are caused by disturbed ciliary assembly, or result from altered ciliary maintenance or disassembly, we focused our analyses on tracheal and bronchial epithelium during early stages of MCC development. First, we monitored expression onset of *Ccno* during lung development (Fig 3A–H). Using the $Ccno^{TA}$ reporter allele, we found first expression in tracheal epithelium at E13, coinciding with the early initiation of MCCs (Fig 3E) (Rawlins *et al*, 2007). During the following

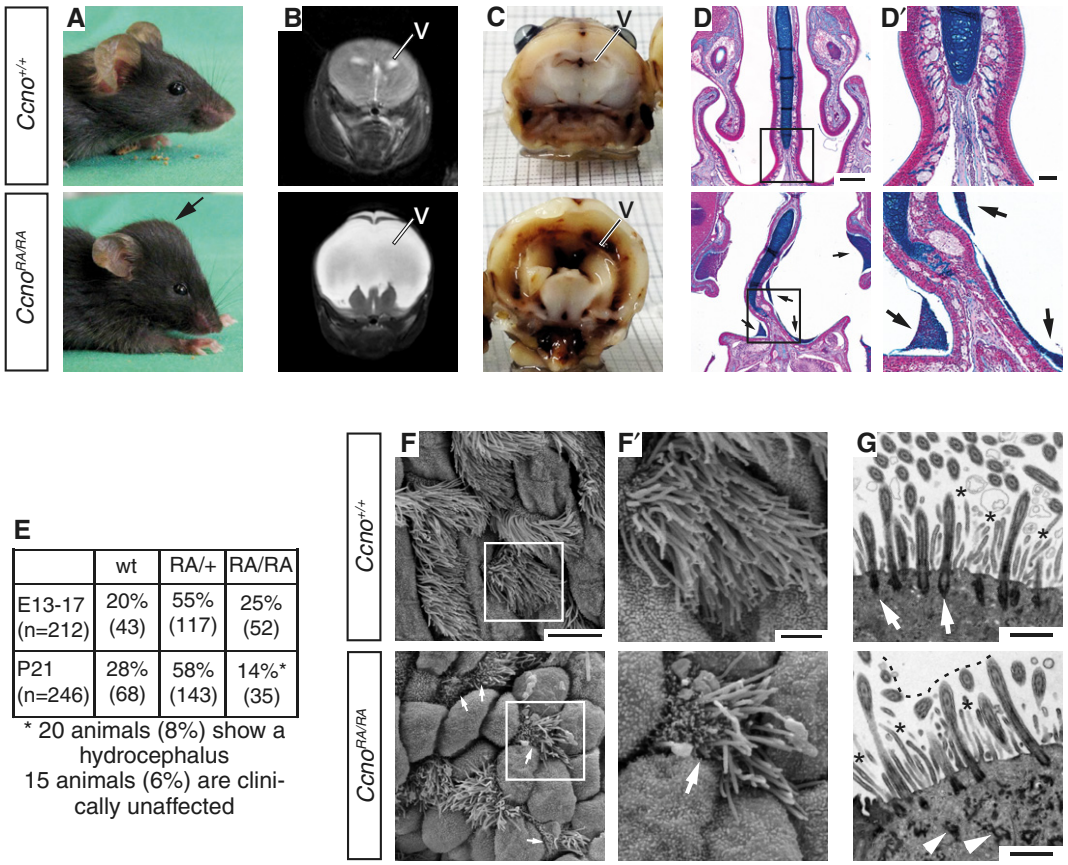

Figure 2. Genetic deletion of *Ccno* leads to severe hydrocephalus, mucociliary clearance deficits and reduced cilia number of MCCs.

A *Ccno*-deficient mice develop severe hydrocephalus resulting in characteristic head deformation at P21 (arrow).

B, C Cranial MRI analysis (B) shows the drastically enlarged ventricular cavity (marked by V) and diminished cerebral cortex tissue, (C) also seen when brains are cut in coronal orientation.

D, D' Alcian-blue staining of paranasal cavities reveals mucus congestion along the nasal epithelium (arrows).

E Survival table of different genotypes at embryonic stages (E13–E17) and at P21 from offspring of heterozygous $Ccno^{RA/+}$ intercrosses. 11% of $Ccno^{RA/RA}$ homozygous animals die between E17 and P21. Of $Ccno^{RA/RA}$ homozygous animals at P21, roughly 60% develop severe hydrocephalus (20/35 animals), and 40% (14/35) appear grossly unaffected.

F, F' Scanning electron microscopy (SEM) of P21 adult trachea shows reduced numbers of cilia of *Ccno*-deficient MCCs. Remaining cilia are found in the central regions of the cell surface, and cell margins frequently lack the ciliary decoration (arrows).

G Transmission electron microscopy (TEM) of wild-type and $Ccno^{RA/RA}$ MCCs from adult trachea. *Ccno*-deficient MCCs show reduced numbers of basal bodies and cilia that correctly docked to the apical cell surface (arrows). Ectopic electron-dense material is found within the cytoplasm of *Ccno*-deficient MCCs (arrowheads).

Data information: Scale bars: 500 μm in (D), 100 μm in (D'), 7 μm in (F), 2 μm in (F') and 1 μm in (G).

developmental stages, *Ccno* expression extended to more distal bronchi. By E16, expression could be found from the trachea to the terminal bronchioles (Fig 3G and H). Thus, *Ccno* expression reflects the spatio-temporal order of MCC development in the respiratory tract (Rawlins *et al*, 2007; Vladar & Stearns, 2007).

To examine stage-dependent *Ccno* expression during ciliogenesis in more detail, we applied mouse tracheal epithelium cell culture (mTEC) techniques (Fig 3I) and compared *Ccno* mRNA expression with transcription of previously described key components for MCC ciliogenesis in wild-type mTECs (Zhao *et al*, 2013). mRNA levels were quantified by qRT–PCR after onset of air–liquid interface culture (ALI) conditions that induces MCC differentiation and ciliogenesis in a semi-synchronized fashion (Fig 3J). Expression profiles of *Deup1*, *Cep152*, *Cep63* and *Ift57* recapitulated published data sets (Zhao *et al*, 2013). *Ccno* mRNA is strongly induced during the first day after onset of ALI conditions and peaked around day 3 (ALI day 3) of differentiation with a 90-fold induction of mRNA levels compared to day 0, thereby paralleling the expression of *Deup1* (Fig 3J). DEUP1 is one of the core components of deuterosomes and becomes upregulated during the early phase of deuterosome formation in mTECs (Zhao *et al*, 2013). The immediate and strong induction of *Ccno* expression at early stages of tracheal epithelium and mTEC differentiation thus suggests that *Ccno*, similar to *Deup1*, may function during the early steps of centriole amplification.

To test if loss of *Ccno* function impacts on the previously described transcriptional programme for deuterosome-dependent (DD) centriole amplification (Ma *et al*, 2014), we performed qRT–PCRs in control and *Ccno*-deficient mTECs (Fig 3K). In wild-type mTECs, key components of DD centriole amplification are strongly induced during the first 3 days of differentiation and expression

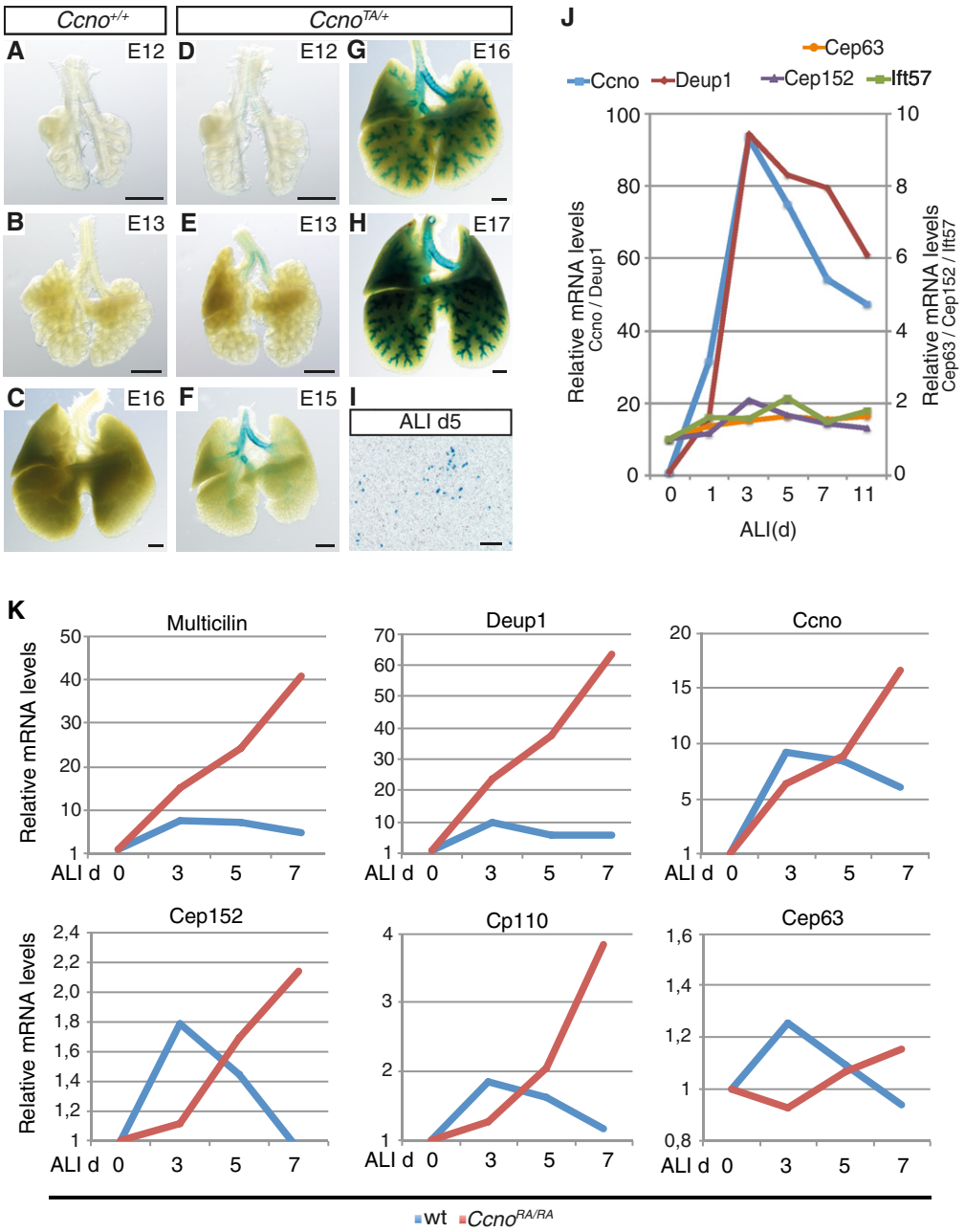

Figure 3. ***Ccno*** **is dynamically expressed from early phases of ciliogenesis and** ***Ccno*** **deficiency impacts on the transcriptional programme for ciliogenesis.**

A–H X-Gal-staining of (A–C) control and (D–H) *Ccno*$^{TA/+}$ embryonic lungs at indicated stages showing onset of *Ccno* expression from E13 in the proximal trachea and in the main bronchi. Expression is extending to more distal regions, and from E16 staining is also found in bronchioli.

I X-Gal-staining indicating *LacZ* expression from the *Ccno*$^{TA/+}$ allele in mTEC cultures after 5 days of differentiation-onset by switching to air–liquid interface (ALI) conditions (ALI d5).

J Transcript levels of *Ccno* and indicated genes with known functions for the generation of multiple cilia during mTEC differentiation. mRNA levels from three independent experiments were measured by qRT–PCR and levels of expression set as 1 on day 0 of ALI cultures. Scales for *Ccno* and *Deup1* are indicated on the left, and for *Cep152*, *Cep63* and *Ift57* on the right side.

K Relative mRNA expression levels for indicated genes were measured by qRT–PCR in wild-type and *Ccno*-deficient mTEC cultures at indicated days after differentiation-onset. Relative values were calculated as in (J) relative to day 0 of ALI cultures.

Data information: Scale bars: 500 μm in (A–H) and 250 μm in (I).

declines shortly afterwards. Recently, it was demonstrated that MULTICILIN is the key transcriptional regulator for the expression of multiple factors for DD centriole amplification, including *Deup1*, *Ccno*, *Cep152* and *Cp110* (Ma *et al*, 2014). In *Ccno*-deficient mTECs, *Multicilin* and all tested downstream targets were strongly induced (Fig 3K) during the first 3 days of differentiation similar to the

wild-type cultures. However, unexpectedly *Ccno*-deficient mTECs failed to downregulate *Multicilin* and other components of the DD pathway after the first induction phase and showed further increasing expression levels until day 7. Interestingly, no increase of *Cep63* expression, a key component for mother-centriole-dependent (MCD) centriole formation, was observed. This could indicate that loss of *Ccno* function specifically impacts on deuterosome-mediated centriole amplification, but not on the MCD pathway.

Ccno-deficient MCCs show ultrastructural and functional defects of deuterosomes and forming centrioles

To analyse functional consequences of *Ccno* deletion at early stages of MCC ciliogenesis in more detail, we performed SEM of tracheal tissue at E17. In contrast to SEM analysis of adult trachea (Fig 2F), we observed a complete absence of multiple cilia on the epithelial surface of *Ccno*-deficient trachea at E17 (Fig 4A–B'). However, ciliogenesis was not generally ablated at this stage in $Ccno^{RA/RA}$ MCCs, since cells with mono- or few cilia with normal morphology could be detected (Fig 4B'). The absence of multiple cilia in E17 tracheal MCCs was also reflected by a significant reduction of acetylated α-tubulin, marking ciliary axonemes (Fig 4C–E). To investigate the underlying cause for the failure to generate multiple cilia, we performed TEM analysis of E17 tracheal epithelium. As expected from SEM, we observed only very few cilia and similarly only few basal bodies that had properly docked to the apical cell membrane in *Ccno*-deficient MCCs (Supplementary Fig S4A and B). At E17, wild-type MCCs frequently exhibited deuterosomes with forming

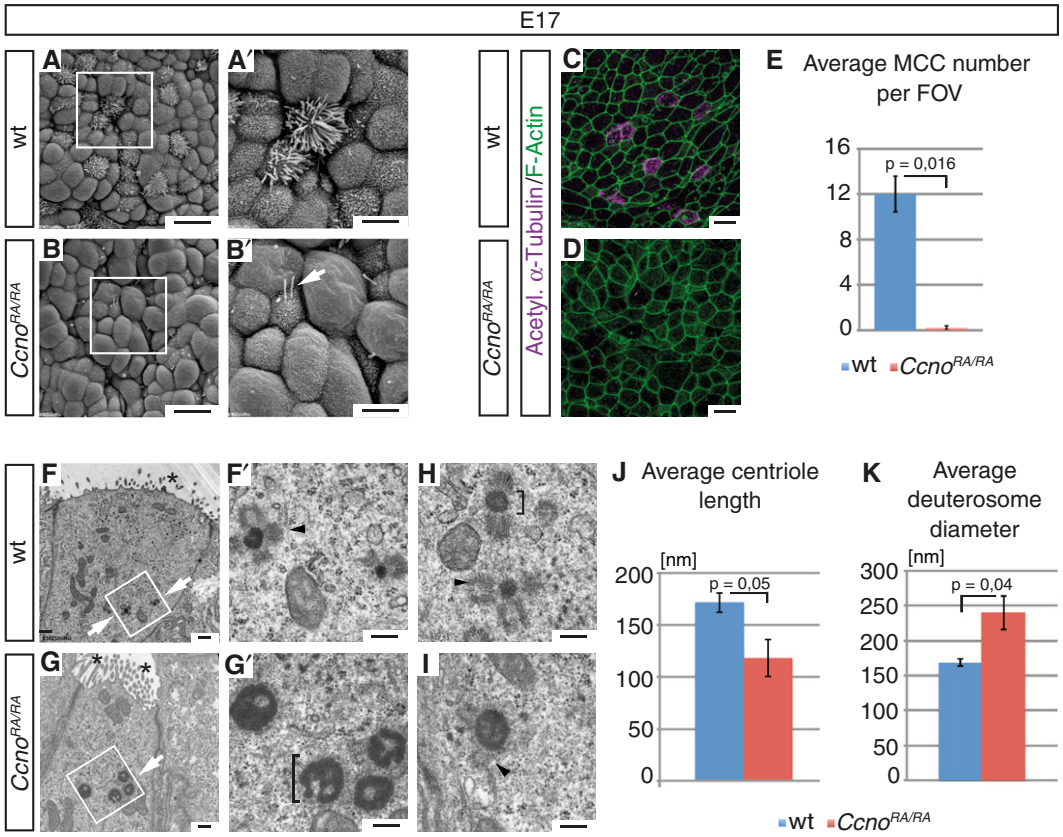

Figure 4. *Ccno*-deficient MCCs at embryonic stages show disturbed ciliogenesis and ultrastructural defects of deuterosome and centrioles.

A–B' SEM of tracheae from (A, A') wild-type and (B, B') $Ccno^{RA/RA}$ embryos at E17. In comparison to wild-type MCCs, *Ccno*-deficient MCCs almost completely lack formation of multiple cilia and only single, or doublet (arrow) cilia are observed at E17.

C–E The lack of multiple cilia at E17 stages is reflected by the almost complete absence of acetylated α-tubulin staining as marker for axonemes in (D) *Ccno*-deficient MCCs of E17 embryonic trachea as quantified in (E). FOV, field of view.

F–I TEM of MCCs from E17 embryonic tracheae shows deuterosomes with forming procentrioles in (F, F', H) *Ccno*-proficient and (G, G', I) *Ccno*-deficient MCCs. Asterisks in (F, G) indicate microvilli that extend from the apical cell surface. (F', G') Deuterosomes in *Ccno*-deficient MCCs are significantly enlarged (identical size bars in F' and G') and show irregular morphology, which is different to the annular shape of wild-type deuterosomes as seen in (F', H). Procentrioles (arrowheads in F' and I) that are found at deuterosomes of (I) *Ccno*-deficient MCCs were recurrently found being shorter and appeared less structured in comparison to (F', H) wild-type cells.

J The average length of procentrioles was quantified for wild-type and Ccno-deficient MCCs of E17 tracheae (49 procentrioles in $n = 3$ independent samples for wild-types and 47 procentrioles in $n = 3$ independent samples for *Ccno*-deficient MCCs).

K The diameter of deuterosomes (41 deuterosomes in $n = 3$ independent samples for wild-types; 38 deuterosomes in $n = 5$ independent samples for *Ccno*-deficient MCCs) was measured in wild-type and *Ccno*-deficient MCCs of E17 tracheae.

Data information: Error bars indicate the standard error of the mean (s.e.m.). *P*-values were calculated by a two-sided Student's *t*-test in (E, J, K). Scale bars: 10 μm in (A, B), 4 μm in (A', B'), 10 μm in (C, D), 500 nm in (F, G) and 200 nm in (F', G'-I).

procentrioles that arrange in a symmetrical fashion surrounding the deuterosome cortex (Fig 4F, F' and H). In striking contrast, deuterosomes of *Ccno*-deficient MCCs only rarely displayed clearly discernable procentrioles (Fig 4G, G' and I), and the few emerging procentrioles were significantly shorter in comparison to controls (Fig 4J). Additionally, the usual symmetrical orientation of centrioles was lost, showing an uneven distribution around the deuterosomes (Fig 4H and I, and Supplementary Fig S4E and E'). As most obvious morphological alteration, the great majority of deuterosomes of *Ccno*-deficient MCCs showed an irregular shape and were significantly enlarged by 42% (Fig 4K) when compared to deuterosomes of wild-type cells (Fig 4F–I and Supplementary Fig S4). Enlarged deuterosomes often showed more than one electron-transparent central region, surrounded by the electron-dense cortex (Fig 4G and G'). In accordance with previous reports (Sorokin, 1968), our TEM analyses confirmed that the deuterosome-dependent (DD) mode represents the predominant way of centriole amplification in tracheal MCCs and deuterosomes outnumbered mother centrioles with forming procentrioles by far. However, mother-centriole-dependent (MCD) centriole amplification could also be found in MCCs of both wild-type and *Ccno*-deficient tracheae at E17 at much lower frequency (Supplementary Fig S4C–D''). In contrast to deuterosomes, these centrioles appeared structurally unaltered and no striking differences between procentrioles of control and *Ccno*-deficient MCCs could be observed (Supplementary Fig S4C–D''). This finding is in accordance with our previous observation by qRT–PCR analysis (Fig 3K) of specific requirements of *Ccno* for DD, but not MCD generation of centrioles.

Formation of deuterosomes and centrioles depends on *Ccno* function

To investigate the formation of deuterosome and centrioles in *Ccno*-deficient MCCs in more detail, we used mTEC cultures followed by IF analysis to mark deuterosomes by staining for DEUP1, and SAS-6 as an early marker for centriole formation (Strnad *et al*, 2007) (Fig 5A). Quantification of IF staining at ALI day 3 revealed an average number of 51 DEUP1-positive deuterosomes with an average diameter of 348 nm in wild-type MCCs (Fig 5C). In *Ccno*-deficient MCCs, deuterosome numbers were significantly reduced to an average of 21 per cell (~60% reduction), while the average deuterosome diameter was enlarged to 515 nm (~48% increase), thus corroborating our previous observations of enlarged deuterosomes by TEM (Fig 4K). This size increase of deuterosomes was further enhanced at later stages of ciliogenesis at ALI day 7 (714 nm), while deuterosome number remained unchanged (19) in *Ccno*-deficient MCCs, but decreased in wild-type MCCs (44) (Fig 5B and C). SAS-6 staining is normally found at the circumference of DEUP1-positive deuterosomes at ALI day 3, indicating the early sites of centriole formation (Zhao *et al*, 2013). In comparison to controls, SAS-6 staining was grossly reduced in *Ccno*-deficient MCCs (Fig 5A), reflecting the generally reduced generation of centrioles, and confirming our previous observation by TEM (Fig 4G and G'). As a result, at later stages of centriole amplification (ALI day 7), Centrin-positive centrioles that predominantly arrange close to the apical surface of wild-type MCCs were dramatically reduced in *Ccno*-deficient cells, and the majority of centrioles was found mislocalized at positions basal to, or at the level of deuterosomes (Fig 5B). Thus, *Ccno* function is required for the proper formation of normal numbers, size and morphology of deuterosomes, and as a consequence, early steps of centriole biogenesis and centriole localization are severely compromised in *Ccno*-deficient cells.

To further quantify centriole formation and to analyse maturation of centrioles, we performed double IF staining for Centrin and CEP164, which marks maturing centrioles during their transition to basal bodies (Graser *et al*, 2007). At ALI day 7, wild-type cells possess ~230 Centrin-positive centrioles, while centriole number was significantly reduced to ~80 in *Ccno*-deficient MCCs (Fig 6A and B). Additionally, the majority of centrioles in *Ccno*-deficient MCCs were not decorated by CEP164-staining, which is normally colocalizing with Centrin at maturing centrioles (Fig 6A). In reverse, IF staining for CP110, which indicates immature centrioles and is normally released from centrioles during maturation and centriole localization to the apical cell surface (Spektor *et al*, 2007; Song *et al*, 2014), showed increased and extended staining in *Ccno*-deficient cells. In contrast, CP110 is normally found only in few MCCs of wild-type mTEC cultures at ALI day 7 (Fig 6C and D). Thus, the significantly reduced staining of CEP164 in combination with retained presence of CP110 demonstrates disturbed maturation of the reduced number of centrioles in *Ccno*-deficient MCCs. Defective centriole maturation is also accompanied by the failure of apical localization of centrioles as seen in z-stack projections (Fig 6A and C).

In summary, *Ccno*-deficient MCCs fail to generate sufficient numbers of functional deuterosomes and consequently form reduced numbers of centrioles. Additionally, the fewer centrioles formed in *Ccno*-deficient MCCs exhibit maturation defects and fail to localize correctly during their transition to basal bodies. As a result, *Ccno*-deficient MCCs show grossly reduced numbers of motile cilia on their apical surface, leading to mucociliary clearance deficits in *Ccno*-deficient animals.

Discussion

This study demonstrates functions of *Ccno* for the deuterosome-mediated generation of multiple motile cilia in MCCs. *Ccno* is very specifically expressed in a dynamic fashion in MCCs, peaking during the earliest phase of deuterosome formation and procentriole generation. The genetic deletion of *Ccno* in mouse leads to the reduced generation of cilia in MCCs, which is most prominent during initial phases of ciliogenesis at embryonic stages. Our ultrastructural and molecular findings suggest specific functions of *Ccno* for the proper formation of deuterosomes and for the deuterosome-dependent generation of procentrioles. Additionally, maturation and apical docking of newly formed centrioles are severely compromised in *Ccno*-deficient MCCs. As a consequence, *Ccno* deficiency causes pleiotropic ultrastructural defects of centrioles, basal bodies and ciliary axonemes and it will be interesting to learn which of these phenotypes are a direct consequence, or secondary effect following loss of *Ccno* function. Additionally, *Ccno* deficiency leads to maintained upregulation of the transcriptional programme that controls centriole amplification, including the key transcriptional regulator *Multicilin* (Ma *et al*, 2014). Maintained expression of factors required for centriole amplification might contribute to the observed phenotype of increased deuterosome size, when the

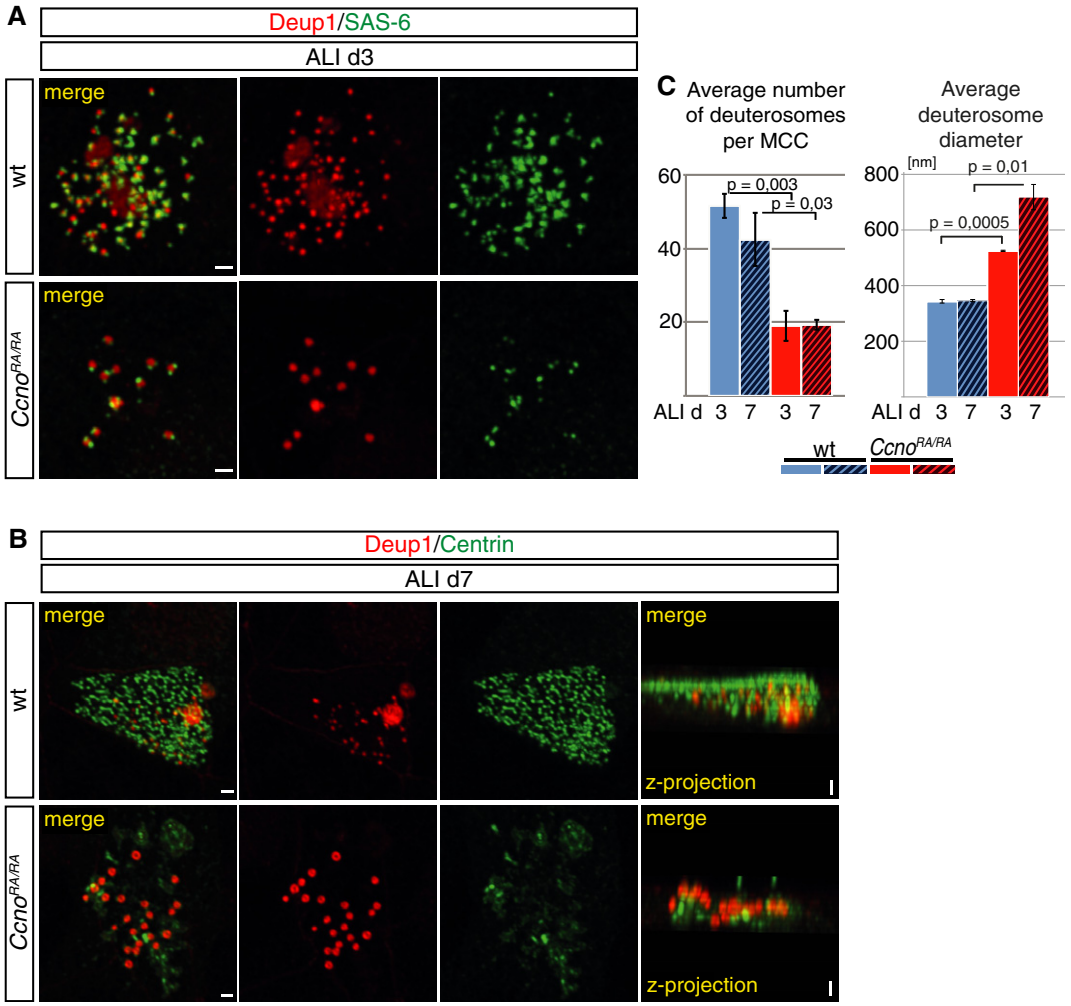

Figure 5. Disturbed deuterosome formation and impaired centriole biogenesis in *Ccno*-deficient MCCs.

A Double IF analysis of mTEC cultures at early stage of MCC differentiation and centriole amplification (ALI day 3) using antibodies for the deuterosome protein DEUP1 and the early centriole marker SAS-6. Deuterosome numbers are decreased and deuterosome size enlarged in *Ccno*-deficient MCCs as quantified in (C). Deuterosome-dependent centriole biogenesis is severely reduced in *Ccno*-deficient MCCs as shown by reduced staining for the early centriole marker SAS-6.

B IF staining for DEUP1 reveals a further size increase of deuterosomes of *Ccno*-deficient MCCs at later stages of centriole biogenesis (ALI day 7). Deuterosome number and size were quantified in (C). IF using a Centrin antibody shows globally reduced presence of centrioles at ALI day 7, which stay localized below the level of deuterosomes and fail to dock to the apical cell membrane in *Ccno*-deficient MCCs as seen in z-projection.

C IF staining for DEUP1 in (A, B) was analysed by Imaris 7.7.2 software to calculate average deuterosome number of wild-type (n = 17) and *Ccno*-deficient (n = 19) MCCs at ALI day 3, and wild-type (n = 12) and *Ccno*-deficient (n = 14) MCCs at ALI day 7. Deuterosome size was measured using the spot measurement tool in n = 10 MCCs for both genotypes at ALI day 3, and in wild-type (n = 12) and *Ccno*-deficient (n = 14) MCCs at ALI day 7.

Data information: Scale bars: 1 μm in all images. Error bars indicate the standard error of the mean (s.e.m.). *P*-values were calculated by a two-sided Student's *t*-test.

duration of deuterosome formation is prolonged. Furthermore, the maintained upregulation of the transcriptional programme for centriole amplification suggests the existence of a regulatory feedback loop that potentially senses centriole number to transcriptionally limit the generation of new centrioles, once sufficient numbers are reached.

Collectively, our observations in mouse extend the range of CCNO functions to earlier stages of centriole amplification, further then previous studies of the cellular phenotype of human individuals with *CCNO* mutations had suggested. Those patients similarly present reduced numbers of cilia of MCCs (Wallmeier *et al*, 2014). However, clinically consequences seem to considerably differ between human and mouse, since hydrocephalus is only rarely found in human individuals and mice do not show obvious respiratory constraints. Similar to human individuals with *CCNO* mutations (Wallmeier *et al*, 2014), and in contrast to previously described PCD patients that entirely fail to form motile cilia (Knowles *et al*, 2013), *Ccno* deficiency in mouse does not cause *situs inversus*, despite highly specific *Ccno* expression in the embryonic node. Elegant studies in mouse had demonstrated that only very few motile cilia in the node are sufficient to break lateral symmetry by unidirectional nodal flow (Shinohara *et al* 2012). Since the ability to form multiple motile cilia is not generally abolished in *Ccno*-deficient embryos, laterality defects are consequently not observed. Further

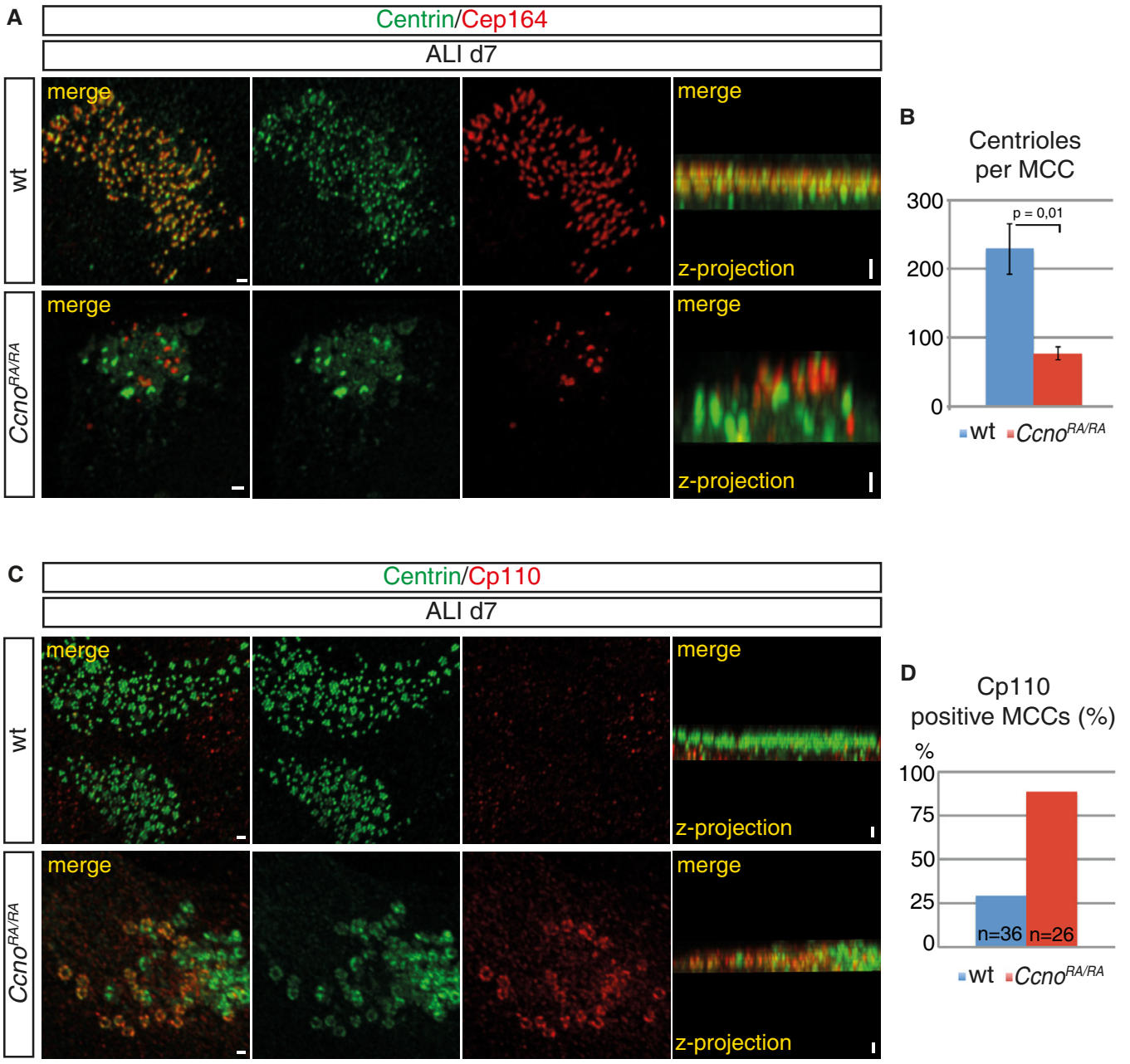

Figure 6. Centriole maturation and localization to the apical cell membrane are defective in *Ccno*-deficient MCCs.

A, B IF analysis of mTEC cultures at ALI day 7 using antibodies against the centriole marker Centrin and CEP164, which marks maturing centrioles. At ALI day 7, centrioles of wild-type MCCs are decorated with CEP164 and are mostly localized to the apical cell membrane. The fewer centrioles of *Ccno*-deficient MCCs do not colocalize with CEP164 and fail to reach the apical cell surface as seen in z-projection. Lack of CEP164 indicates immature centrioles in *Ccno*-deficient MCCs. (B) Total centriole numbers per MCC were counted in $n = 11$ MCCs for both genotypes using Imaris 7.7.2 software.

C, D Double IF staining using Centrin- and CP110-specific antibodies shows an almost complete absence of CP110 from Centrin-positive centrioles in the majority of wild-type MCCs at day 7 of ALI cultures. Most *Ccno*-deficient MCCs exhibit pronounced CP110 staining that colocalizes with Centrin as seen in z-projection. (D) CP110-positive MCCs were counted in wild-type and *Ccno*-deficient MTEC cultures and the percentages of CP110-positive MCCs from total MCCs calculated.

Data information: Scale bars: 1 μm in all images. Error bars indicate the standard error of the mean (s.e.m.). *P*-values were calculated by a two-sided Student's *t*-test.

studies will be required to shed light on *Ccno* functions in the mono-ciliated cells of the embryonic node.

Cyclins most frequently act by regulating cyclin-dependent kinases (CDKs). While kinases or other molecular targets that are controlled by *Ccno* remain to be defined, their identification may provide fundamental insights into regulation of deuterosome-mediated centriole amplification. It is tempting to speculate that *Ccno,* which is specifically expressed in MCCs, underwent a functional switch from promoting cell cycle progression to adopting a new role during deuterosome-dependent amplification of centrioles. Both

processes, centriole duplication during S-phase in cycling cells and centriole amplification at deuterosomes of MCCs, use in parts the same regulatory machinery that might be redirected by *Ccno* functions in MCCs (Klos Dehring *et al*, 2013; Zhao *et al*, 2013).

The precise molecular action of CCNO currently remains unresolved. Thus, it will be interesting to learn if the various defects at multiple stages of centriole biogenesis in *Ccno*-deficient MCCs are caused by different, possibly independent CCNO functions, or if all defects arise from disturbances of one common cellular process that is coordinated by CCNO. One example of such an overreaching process could be the spatio-temporal control of microtubular and/or actin-based trafficking of deuterosome or centriole components. Disturbances hereof could simultaneously impact on the formation of deuterosomes and on the different steps of ciliogenesis, for example the generation, maturation and localization of centrioles. These different steps of ciliogenesis are normally executed in a highly synchronized manner that involves all centrioles of a cell during MCC ciliogenesis (Al Jord *et al*, 2014). Our data indicate that at least one step, namely the maturation of centrioles, is not fully synchronized in *Ccno*-deficient MCCs, since the presence of different maturation stages of centrioles can be observed in the same cell. Further molecular analyses and dynamic imaging of centriole biogenesis in *Ccno*-deficient MCCs will allow unveiling *Ccno*-dependent regulation of deuterosome function during centriole amplification.

Materials and Methods

Mouse tracheal epithelial cell (mTEC) culture

mTECs were isolated from wild-type, $Ccno^{TA/+}$ or $Ccno^{RA/RA}$ mice at 6 weeks of age or older, as described previously (You *et al*, 2002; Vladar & Brody, 2013). In brief, tracheal epithelial cells were isolated by overnight pronase digestion at 4°C and separated on the following day from contaminating fibroblasts by a 3- to 4-h incubation on a Primaria cell culture plate in mTEC basal medium (Vladar & Brody, 2013). mTECs were seeded on collagen-coated apical chambers of Transwell-Clear filters. Proliferation medium (Vladar & Brody, 2013) was applied to the apical and basal chamber of the transwells and cells cultured at 37°C, 5% CO_2. Air–liquid interface (ALI) culture conditions were applied after 6 days of culture by removal of the medium from the apical chamber. Additionally, differentiation was initiated by exchange of proliferation medium with differentiation medium (basal medium + 50 nM retinoic acid + 2% NuSerum).

Immunofluorescence staining of mTEC cultures

mTEC cultures were briefly washed with PBS and fixed in 4% PFA for 15 min at RT, washed with PBS containing 0.1% Triton X (PBX) and blocked for 1 h in PBX containing 4% bovine serum albumin (BSA) and 10% foetal bovine serum (FBS). mTEC cultures were incubated with primary antibody in blocking solution for 1.5 h at RT, using the antibodies listed in Supplementary Table S1. After washing, samples were incubated in PBX for 45 min at RT with conjugated secondary antibody as listed in Supplementary Table S1. mTEC filters were mounted with ProLong Diamond Antifade Mountant (Life technologies P36961) and fluorescent images were captured with a Zeiss inverted laser-scanning microscope (LSM 510 Meta), equipped with a 1.4×/100× Plan-Apochromat objective. Image stacks were recorded with a z-distance of 0.38 μm and subjected to Huygens deconvolution, using Huygens remote manager (hrm) software. Displayed images are snapshots taken from the 3-D surpass display mode of Imaris 7.2.2 software after Huygens deconvolution. For all images used for figure assembly, the brightness was equally increased from 0 to 20, using Adobe Photoshop CS6.

Analysis and statistics for immunofluorescence of mTEC cultures

After Huygens deconvolution, images were analysed with Imaris 7.7.2 software. For calculations of the mean diameter, 7–10 deuterosomes were measured at the z-plane of their largest diameter in the 2D-Slice display mode. Mean diameters of $n = 10$ cells at ALI day 3 (wild-type and $Ccno^{RA/RA}$ cells) and $n = 12$ (wild-type), and $n = 14$ ($Ccno^{RA/RA}$) cells at ALI day 7 were measured. Average deuterosome number was analysed in the 3D-Surpass display mode, using the spot measurement tool. Estimated spot diameter was based on the mean deuterosome diameter calculated per cell in the previous analysis. Mean deuterosome number per cell was calculated from $n = 17$ (wild-type) and $n = 19$ ($Ccno^{RA/RA}$) cells at ALI day 3, and $n = 12$ (wild-type) or $n = 14$ ($Ccno^{RA/RA}$) cells at ALI day 7. For analysis of average centriole number, those *Ccno*-deficient cells were chosen that showed clearly discernible centriolar structures, due to increased heterogeneity of Centrin IF staining in *Ccno*-deficient cells when compared to wild-type cells. Measurement of centrioles was performed as described for deuterosome number ($n = 11$ cells for wild-type and $Ccno^{RA/RA}$) at ALI day 7. For statistical analysis, a two-sided Student's *t*-test (*P*-value indicated on respective graph) was applied and the standard error of the mean (s.e.m.) was calculated for each data set individually.

Scanning and transmission electron microscopy

For electron microscopy, tissues were fixed in 2.5% glutaraldehyde, 2% PFA and 0.1% picric acid in 0.1 M phosphate buffer pH 7.0 followed by washes in 0.1 M phosphate buffer pH 7.0. Processing for transmission electron microscopy (TEM) included postfixation with an aqueous solution of 1% osmiumtetroxide for 1 h, washes in distilled H_2O and processing through an increasing acetone series to 100% acetone, followed by infiltration with epoxy resin (Epon 812, Serva, Heidelberg, Germany) starting in a 1:1 mixture of acetone and resin o/n, followed by pure resin for 4 h. Specimens were transferred to rubber moulds and cured at 60°C for 2 days. Resin blocks were trimmed using the Leica EM Trim 2 (Leica Microsystems, Wetzlar, Germany). Semithin sections (approximately 0.5 μm) and thin sections (50–70 nm) were cut on a ultramicrotome (Ultracut S, Reichert, Wien, Austria) with a diamond knife (Diatome, Biel, Switzerland). Semithin sections were stained with toluidine blue to visualize areas for thin sectioning and ultrastructural inspection. Thin sections were transferred to copper grids and stained with uranyl acetate and lead citrate and were examined on a Zeiss EM902 electron microscope operated at 80 kV (Carl Zeiss, Oberkochen, Germany). Digital images were acquired with a side-mounted 1x2k FT-CCD Camera (Proscan, Scheuring, Germany) using iTEM camera control and imaging software (Olympus Soft Imaging Solutions, Münster, Germany).

For scanning electron microscopy (SEM), tissues were dehydrated with a graded series of either ethanol or acetone, followed by immersion in CO_2 and subsequent critical point drying in a Emitech K850 critical point dryer (Emitech Ltd. Ashford, UK). Specimens were mounted on SEM stubs with adhesive carbon tape (Plano, Wetzlar, Germany) and sputter-coated with a gold layer (approximately 15–20 nm thickness) using a Bal-Tec SCD004 sputter coater (Balzers Union Ltd., Balzers, Liechtenstein). Specimens were viewed on a Zeiss DSM960A SEM equipped with digital image scanning and processing systems and software (Point Electric, Halle, Germany) operated at 10–20 kV and in a field-emission SEM Zeiss Merlin VP compact operated at 10 kV. Images with a size of 512×512 and 1000×1000 pixels (DSM960A) and 1024×768 pixels (Merlin VP compact) were recorded.

Morphometric measurements and quantification of TEM

The diameter of deuterosomes and length of procentrioles attached to deuterosomes were separately analysed on the same sets of TEM micrographs from E17.5 wild-type ($n = 3$) and *Ccno*-deficient ($n = 5$) embryonic trachea specimens using the free line measurement tool in the iTEM imaging software. The annotated values from each picture were exported into Microsoft Excel-compatible tables using the export function of the iTEM software. For deuterosomes, all clearly identifiable deuterosomes on the pictures obtained from the specimens were measured across for their largest diameter, in total $n = 41$ wild-type and $n = 38$ *Ccno*-deficient deuterosomes. For procentriole length, the largest visible length of the procentriole perpendicular to the deuterosome was measured and only procentrioles on deuterosomes bearing two or more clearly visible procentrioles were taken into account. A total of 49 wild-type (in $n = 3$ independent samples) and $n = 47$ *Ccno*-deficient (in $n = 3$ independent samples) procentrioles were measured. For statistical analysis, both data sets (wt and *Ccno*-deficient) of deuterosome diameters and centriole length were applied to a two-sided Student's *t*-test (*P*-values indicated on respective graph).

Animals

All mice were housed in the pathogen-free barrier facility of the University Medical Centre Freiburg in accordance with the institutional guidelines and approval by the regional board.

Additional Material and Methods including tables of antibodies and primers can be found in the Supplementary Information.

Supplementary information for this article is available online: http://emboj.embopress.org

Acknowledgements

We thank Petra Pennekamp, Niki Tomas Loges und Julia Wallmeier for video microscopy and IF; Ute Schulz, Wolfgang Labs and Gerhard Fulda for technical assistance with SEM/TEM; Wilfried Reichardt for MRI analysis; Sarah Dräger and Hannes Engel for help during *in situ* expression screening; Barbara Müller and Simone Bräg for technical assistance of lentiviral transduction; Roland Nitschke and the Freiburg Life Imaging Centre (LIC) for supervision of confocal microscopy; Erich Nigg and Xiumin Yan for antibodies; and Alexis Hofherr, Miriam Schmidts, Simone Probst, Michael Köttgen and Gerd Walz for thoughtful discussions and comments on the manuscript. This work was supported by the Emmy Noether Programme of the German Research Foundation (DFG) to SJA (AR732/1-1), BIOSS Centre of Biological Signalling Studies to SJA and the Excellence Initiative of the German Research Foundation (GSC-4, Spemann Graduate School).

Author contributions

MCF and SJA conceived the study, performed experiments and analysed the data. ANB, GK, KT and SSL assisted and supervised some experiments. TM performed IF analyses and video microscopy of tracheal and ependymal epithelium. MF performed, analysed and interpreted electron microscopy. JD and HO helped with data analysis and during writing of the manuscript. MCF assembled the figures, SJA wrote the manuscript, and SJA and MCF edited the manuscript.

Conflict of interest

The authors declare that they have no conflict of interest.

References

Al Jord A, Lemaitre AI, Delgehyr N, Faucourt M, Spassky N, Meunier A (2014) Centriole amplification by mother and daughter centrioles differs in multiciliated cells. *Nature* 516: 104 – 107

Blachon S, Gopalakrishnan J, Omori Y, Polyanovsky A, Church A, Nicastro D, Malicki J, Avidor-Reiss T (2008) Drosophila asterless and vertebrate Cep152 Are orthologs essential for centriole duplication. *Genetics* 180: 2081 – 2094

Brody SL, Yan XH, Wuerffel MK, Song SK, Shapiro SD (2000) Ciliogenesis and left-right axis defects in forkhead factor HFH-4-null mice. *Am J Respir Cell Mol Biol* 23: 45 – 51

Carvalho-Santos Z, Azimzadeh J, Pereira-Leal JB, Bettencourt-Dias M (2011) Evolution: tracing the origins of centrioles, cilia, and flagella. *J Cell Biol* 194: 165 – 175

Chen J, Knowles HJ, Hebert JL, Hackett BP (1998) Mutation of the mouse hepatocyte nuclear factor/forkhead homologue 4 gene results in an absence of cilia and random left-right asymmetry. *J Clin Invest* 102: 1077 – 1082

Fliegauf M, Olbrich H, Horvath J, Wildhaber JH, Zariwala MA, Kennedy M, Knowles MR, Omran H (2005) Mislocalization of DNAH5 and DNAH9 in respiratory cells from patients with primary ciliary dyskinesia. *Am J Respir Crit Care Med* 171: 1343 – 1349

Fliegauf M, Benzing T, Omran H (2007) When cilia go bad: cilia defects and ciliopathies. *Nat Rev Mol Cell Biol* 8: 880 – 893

Graser S, Stierhof YD, Lavoie SB, Gassner OS, Lamla S, Le Clech M, Nigg EA (2007) Cep164, a novel centriole appendage protein required for primary cilium formation. *J Cell Biol* 179: 321 – 330

Hayashi S, Lewis P, Pevny L, McMahon AP (2002) Efficient gene modulation in mouse epiblast using a Sox2Cre transgenic mouse strain. *Mech Dev* 119 (Suppl 1): S97 – S101

Kleylein-Sohn J, Westendorf J, Le Clech M, Habedanck R, Stierhof YD, Nigg EA (2007) Plk4-induced centriole biogenesis in human cells. *Dev Cell* 13: 190 – 202

Klos Dehring DA, Vladar EK, Werner ME, Mitchell JW, Hwang P, Mitchell BJ (2013) Deuterosome-mediated centriole biogenesis. *Dev Cell* 27: 103 – 112

Knowles MR, Daniels LA, Davis SD, Zariwala MA, Leigh MW (2013) Primary ciliary dyskinesia. Recent advances in diagnostics, genetics, and characterization of clinical disease. *Am J Respir Crit Care Med* 188: 913 – 922

Lee L (2013) Riding the wave of ependymal cilia: genetic susceptibility to hydrocephalus in primary ciliary dyskinesia. *J Neurosci Res* 91: 1117 – 1132

Ma L, Quigley I, Omran H, Kintner C (2014) Multicilin drives centriole biogenesis via E2f proteins. *Genes Dev* 28: 1461 – 1471

Nigg EA, Raff JW (2009) Centrioles, centrosomes, and cilia in health and disease. *Cell* 139: 663 – 678

Rawlins EL, Ostrowski LE, Randell SH, Hogan BL (2007) Lung development and repair: contribution of the ciliated lineage. *Proc Natl Acad Sci USA* 104: 410 – 417

Shinohara K, Kawasumi A, Takamatsu A, Yoshiba S, Botilde Y, Motoyama N, Reith W, Durand B, Shiratori H, Hamada H (2012) Two rotating cilia in the node cavity are sufficient to break left-right symmetry in the mouse embryo. *Nat Commun* 3: 622

Shiratori H, Hamada H (2006) The left-right axis in the mouse: from origin to morphology. *Development* 133: 2095 – 2104

Skarnes WC, Rosen B, West AP, Koutsourakis M, Bushell W, Iyer V, Mujica AO, Thomas M, Harrow J, Cox T, Jackson D, Severin J, Biggs P, Fu J, Nefedov M, de Jong PJ, Stewart AF, Bradley A (2011) A conditional knockout resource for the genome-wide study of mouse gene function. *Nature* 474: 337 – 342

Song R, Walentek P, Sponer N, Klimke A, Lee JS, Dixon G, Harland R, Wan Y, Lishko P, Lize M, Kessel M, He L (2014) miR-34/449 miRNAs are required for motile ciliogenesis by repressing cp110. *Nature* 510: 115 – 120

Sorokin SP (1968) Reconstructions of centriole formation and ciliogenesis in mammalian lungs. *J Cell Sci* 3: 207 – 230

Spektor A, Tsang WY, Khoo D, Dynlacht BD (2007) Cep97 and CP110 suppress a cilia assembly program. *Cell* 130: 678 – 690

Strnad P, Leidel S, Vinogradova T, Euteneuer U, Khodjakov A, Gonczy P (2007) Regulated HsSAS-6 levels ensure formation of a single procentriole per centriole during the centrosome duplication cycle. *Dev Cell* 13: 203 – 213

Tang TK (2013) Centriole biogenesis in multiciliated cells. *Nat Cell Biol* 15: 1400 – 1402

Vladar EK, Stearns T (2007) Molecular characterization of centriole assembly in ciliated epithelial cells. *J Cell Biol* 178: 31 – 42

Vladar EK, Brody SL (2013) Analysis of ciliogenesis in primary culture mouse tracheal epithelial cells. *Methods Enzymol* 525: 285 – 309

Wallmeier J, Al-Mutairi DA, Chen CT, Loges NT, Pennekamp P, Menchen T, Ma L, Shamseldin HE, Olbrich H, Dougherty GW, Werner C, Alsabah BH, Kohler G, Jaspers M, Boon M, Griese M, Schmitt-Grohe S, Zimmermann T, Koerner-Rettberg C, Horak E *et al* (2014) Mutations in CCNO result in congenital mucociliary clearance disorder with reduced generation of multiple motile cilia. *Nat Genet* 46: 646 – 651

You Y, Richer EJ, Huang T, Brody SL (2002) Growth and differentiation of mouse tracheal epithelial cells: selection of a proliferative population. *Am J Physiol Lung Cell Mol Physiol* 283: L1315 – L1321

Zhao H, Zhu L, Zhu Y, Cao J, Li S, Huang Q, Xu T, Huang X, Yan X, Zhu X (2013) The Cep63 paralogue Deup1 enables massive de novo centriole biogenesis for vertebrate multiciliogenesis. *Nat Cell Biol* 15: 1434 – 1444